



Published in final edited form as:

*Colloids Surf B Biointerfaces*. 2019 October 01; 182: 110300. doi:10.1016/j.colsurfb.2019.06.030.

## Small Molecule Delivery Across a Perforated Artificial Membrane by Thermoreversible Hydrogel Poloxamer 407

A. Santimetaneedol<sup>1</sup>, Z. Wang<sup>1</sup>, D. N. Arteaga<sup>2</sup>, A. Aksit<sup>1</sup>, C. Prevotau<sup>2</sup>, M. Yu<sup>2</sup>, H. Chiang<sup>2</sup>, D. Fafalis<sup>1</sup>, A. K. Lalwani<sup>\*,1,2</sup>, J. W. Kysar<sup>1,2</sup>

<sup>1</sup>Department of Mechanical Engineering, Columbia University, New York, NY

<sup>2</sup>Department of Otolaryngology–Head & Neck Surgery, Columbia University Medical Center, New York, NY

### Abstract

Microperforations in the round window membrane have been suggested for enhancing the rate and reliability of drug delivery into the cochlea. Intratympanic injection, the most common delivery method, involves injecting therapy into the middle ear to establish a reservoir from which drug diffuses across the round window membrane into the cochlea. This process is highly variable because (i) the reservoir, if liquid, can lose contact with the membrane and (ii) diffusion across the membrane is intrinsically variable even with a stable reservoir. To address these respective sources of variability, we compared the thermoreversible hydrogel poloxamer 407 (P407) to saline as a drug carrier and studied the effect of membrane microperforations on drug diffusion rate. We used Rhodamine B as a drug proxy to measure permeance across an artificial membrane in a horizontal diffusion cell. We found that permeance of Rhodamine B from a saline reservoir was an order of magnitude higher than that from a P407 reservoir across unperforated membranes. Moreover, permeance increased with total perforation cross-sectional area regardless of number of perforations ( $p < 0.05$  for all saline-based experiments), but the same association was not found with P407. Rather, for a P407 reservoir, only a large perforation increased permeance ( $p < 0.001$ ), while multiple small perforations did not ( $p = 0.749$ ). These results confirm that for drug dissolved in saline, multiple small perforations can effectively enhance diffusion. However, for drug dissolved in P407, larger perforations are necessary.

### Keywords

Poloxamer 407; Rhodamine B; Diffusion Test; Franz Cell; Valia-Chien Cell; Drug Delivery; Intratympanic (IT) Injection; Round Window Membrane

## 1 Introduction

Microperforations are emerging as an effective drug delivery method across a wide variety of fields in medicine and pharmacology. They have been suggested as a means to enhance the treatment of diseases affecting the cochlea such as sudden sensorineural hearing (SSNH)

\*Corresponding Author: ak12144@cumc.columbia.edu.

loss and Ménière's disease, for which treatment options have been associated with inconsistent drug delivery and frequent side effects [1-3]. Currently, the most common treatment for these disorders is intratympanic injection (cf. Fig. 1), during which liquid glucocorticoid or gentamicin is delivered via needle and syringe through the tympanic membrane and into the middle ear [4, 5]. The injected therapeutic diffuses across the round window membrane—a thin tissue separating the inner and middle ear compartments—and into the diseased cochlea. However, intratympanic (IT) dosing suffers from two flaws inherent to the technique. First, diffusion of drug into the cochlea depends on the time of contact between the therapeutic agent and the RWM [6, 7]. While contact is maintained when the patient is lying down, liquid therapeutic is inevitably lost via the Eustachian tube once the patient sits upright. Second, the rate of molecular transport across the round window membrane (RWM) itself is highly variable [6, 8-11]. Thus, there is a critical need for new tools to improve upon the existing IT dosing technique and to reduce the variability in drug delivery to the cochlea.

In an attempt to overcome these challenges, investigators have tested novel surgical approaches for precise delivery of therapeutic agents into the inner ear, including the use of a wide variety of microinjection, microperforation and continuous infusion devices [12-15]. Our laboratory in particular, has explored the use of microneedle technology for the diagnosis and treatment of diseases through the RWM [16, 17]. We have fabricated needles, based on a microanatomic analysis of guinea pig RWM, that can create precise microperforations *in vitro* for enhancing drug diffusion [16, 18]. Our technology also allows us the flexibility to create many needles of other designs for various purposes [18]. Our needles can: (1) precisely create small (or large) perforations without tearing the RWM, (2) sample fluids from across the RWM for diagnostic purposes, and (3) detect successful perforation of the RWM without relying on direct visualization [18-21].

A critical adjunct to microneedle-based drug delivery to the inner ear is the development of sustained-release drug formulations that minimize the variability in a perilymph pharmacokinetic profile. Of particular interest in recent years due to its thermosensitive properties, the hydrogel poloxamer 407 is liquid when kept cool, but transforms into a semi-solid hydrogel at higher temperatures [22-26]. This gelification phenomenon is reversible, and higher poloxamer 407 (P407) concentrations result in lower transition temperatures and greater gel strength [27]. P407 acquires its unique physical traits from a combination of distinct hydrophilic and hydrophobic blocks, whose solubilities in water are temperature dependent; its chemical structure is as follows:



Because drugs and other solutes can be dissolved into liquid P407 solutions without significantly inhibiting gelification, P407 has been extensively studied as a vehicle for pharmaceutical delivery to the ear [27-29]. Via conventional IT dosing, a room-temperature P407-based solution containing otologic therapy can be injected into the middle ear space, where body temperature triggers transformation of the mixture into a gel. In turn,

gelification can prolong the residence time of the injected solution and maintain contact between the drug and the RWM. In humans, a P407-based antibiotic formulation (OTIPRIO®; Otonomy, Inc) administered via IT injection has been approved for the treatment of middle ear infections [30]. These infections affect structures immediately adjacent to the cochlea, so there is reason to believe that this drug delivery technique can also be applied to inner ear disease. Indeed, animal studies have demonstrated that P407-based dexamethasone formulations, delivered via IT injection, allow for sustained-release drug delivery to the cochlea [23-25].

The research described in this correspondence explores a novel method for enhancing IT injection techniques for more effective and consistent drug delivery across the RWM and into the cochlea. Previously, our laboratory has demonstrated that a single microscopic perforation can increase the rate of material diffusion across the guinea pig RWM *in vitro* from a saline reservoir [15]. We hypothesize that multiple microperforations with a large total cross-sectional area will further augment diffusive transport. Compared to a single large perforation in the RWM, multiple microperforations with the same total cross-sectional area could be advantageous because holes of smaller diameter exhibit higher viscous resistance to fluid flow, simultaneously enhancing diffusive transport of therapeutic reagents into the cochlea and reducing outward leakage of perilymph. However, the contribution of multiple microperforations to cochlear drug delivery remains experimentally unknown. Moreover, the interaction between microperforations and novel gelatinous drug carriers is unclear. Answering these questions will have far-reaching implications for drug delivery across other thin anatomical membranes, such as those found in the eye and central nervous system. Herein we investigate the role of multiple microscopic perforations as an adjunct to prolonged therapeutic delivery by gelatinous drug carriers as compared with conventional saline solution.

## 2 Methods

We use a Valia-Chien cell apparatus separated by an artificial barrier membrane to compare the *in vitro* drug delivery kinetics of the small molecule Rhodamine B delivered via P407 and saline solution, both with and without perforations. The applied methods for measuring trans-membrane diffusion were adapted from the American Association of Pharmaceutical Scientists as well as the Federal Drug Administration recommendations for *in vitro* percutaneous absorption rate studies [31].

### 2.1 Media and Components

Rhodamine B (RhoB) ( $479.01 \text{ g mol}^{-1}$ ,  $\log P_{\text{OW}} 1.95$ , >99% purity; ACROS 29657) is a fluorescent tracer that can be rapidly and accurately quantified with fluorescent microscopy (Acros Organics, Pittsburgh, PA). RhoB has previously been used as a proxy for relevant otologic therapies and has a molecular weight comparable to that of gentamicin [15, 32]. A solution of 0.10mM RhoB dissolved in phosphate-buffered saline (PBS) was used as the therapeutic proxy for 40 mg mL<sup>-1</sup> solution of gentamicin (0.08 mM), a common concentration used in IT injections for the treatment of Ménière's disease [3]. In what follows, we use the terms PBS and saline interchangeably.

We mixed P407 powder (Spectrum Chemical, Gardena, CA) with demineralized water and RhoB to create a 0.1mM RhoB solution in 18% P407 by weight. The resulting mixture was stirred at room temperature and kept overnight in a refrigerator at 3 to 4°C to facilitate dissolution of the P407 powder. At the chosen P407 concentration, the mixture transitioned into gel upon placement within the room-temperature testing apparatus.

## 2.2 Diffusion Cells

Diffusion of RhoB through an artificial membrane barrier was performed using 9mm clear unjacketed Valia-Chien diffusion cells (PermeGear Inc., Hellertown, PA) with 5mL volumes and flat-ground joints. The cell, as shown in Fig. 2, consists of three parts: (1) a donor half-cell, (2) a receptor half-cell, and (3) an artificial membrane barrier separating the two. The Valia-Chien diffusion cells were arranged horizontally, mitigating the effects of gravity on particle movement and allowing for active stirring of both the donor and receptor compartments by magnetic mini-stirrers (HI 190M-1, Hanna Instruments, Woonsocket, RI) [33].

The donor chamber was filled with 5.0mL volumes of: (A) 0.1mM RhoB in PBS or (B) 0.1 mM RhoB in 18% P407. An additional sample of donor solution was reserved for the calibration of fluorescence detection, as detailed below. Active stirring of the donor chamber was performed for experiments utilizing PBS, but not those utilizing gelified P407. Initial filling of the donor chamber marked time zero for each experiment.

The receptor chamber was filled with 5.0mL of PBS prepared by dissolving 9.6g of Dulbecco's Phosphate Buffered Saline powder (Sigma-Aldrich) in 1.0L deionized water. An Eppendorf micropipette was used to withdraw 75  $\mu$ L of fluid from the receptor chamber every 15 min, from 0 min to 165 min, for a total of 12 samples. The collected samples were placed in individual wells of a 96-well plate for further analysis. The withdrawn solution was replaced with 75  $\mu$ L of PBS to prevent advection of fluid within the system. The concentration in the receptor chamber was significantly lower than that in the donor chamber for the entirety of experiments; as such, this process had minimal effect on subsequent measurements of donor chamber concentrations. Active stirring of the receptor chamber was performed for all experiments.

Whatman™ Grade 2 Qualitative Filter Paper with diameter 5.5 cm, thickness 190  $\mu$ m and pore size 8.0  $\mu$ m (Whatman Limited, England) was used as an artificial membrane barrier separating the donor and receptor chambers. This filter paper was used as a proxy for anatomical membranes such as the RWM, which experimentally exhibits highly variable thickness and permeability [6, 8-11]. Using an artificial barrier controlled for pore size as well as membrane thickness. The filter paper was cut to fit a custom 3D-printed diffusion cell adapter, which was circumferentially sealed with general-purpose epoxy. Teflon tape was used to prevent leakage between the 3D-printed adapter and the joint, which were secured with a standard Valia-Chien cell clamp. The filter paper was equilibrated in PBS solution for 30 min prior to any contact with donor substance. Microperforations were introduced in the filter paper with manual application of a stainless steel minuten insect pin with diameter tip of 12.5  $\mu$ m and diameter shaft of 100  $\mu$ m and 200  $\mu$ m (Austerlitz, Czech Republic) under a stereoscopic microscope. Imaging by 3D digital microscope was used to

confirm the presence and sizing of perforations in the filter paper (Fig. 3a). Original MATLAB code was written to measure the area of the exposed portion of the filter paper barrier, which varied with leakage of epoxy from the diffusion cell adapter (Fig. 3b). A summary of all experimental setups, differing by solvent and size and number of perforations, is described in Table 1.

### 2.3 Fluorescence Detection

Samples from each time point were analyzed for relative RhoB concentration by detection with fluorescent microscopy. These samples were diluted with PBS by a factor of 10 to prevent gelification of the solution prior to fluorescent microscopy. A 96-well plate containing 13 samples (1 reference sample from the donor chamber and 12 samples from the receptor chamber) was analyzed using a Synergy™ 4 BioTek Multi-Detection Microplate Reader (BioTek, Winooski, VT) with excitation and emission wavelengths set to 554 nm and 590 nm, respectively. Calibration curves were constructed using standards of RhoB concentrations between 0.01  $\mu\text{M}$  and 10.0  $\mu\text{M}$ .

### 2.4 Quantitative Methods

The experiments described above can be modeled mathematically according to equations derived from Fick's second law of diffusion. Combining the equations for unsteady state mass transfer between two chambers and for steady state flux across a membrane leads to an approximate solution for our experiments. This solution holds for thin membrane such as ours where the membrane quickly reaches its steady state condition [34].

In the steady state condition of the membrane, not to be confused with the steady state condition of the two chambers, the flux across the membrane is proportional to the concentration difference between the two chambers such that

$$j_{\text{RhoB}} = k_p(C_D - C_R) \quad (1)$$

where  $j_{\text{RhoB}}$  is the flux at the interface expressed in concentration per area per time [ $\text{m}^{-2}\text{s}^{-1}$ ],  $C_D$ ,  $C_R$  are the RhoB concentrations per volume [ $\text{m}^{-3}$ ] in the donor and receptor chambers, respectively, and  $k_p$  is the membrane permeance of RhoB in dimensions of velocity [ $\text{m/s}$ ].

The mass balance equations of the Valia-Chien chambers are

$$V \frac{dC_D}{dt} = -A j_{\text{RhoB}} \quad (2a)$$

$$V \frac{dC_R}{dt} = +A j_{\text{RhoB}} \quad (2b)$$

where  $A$  is the membrane's area and  $V$  the volume of each chamber (both the same in our case). Dividing these mass balances by the chambers' volume  $V$ , subtracting the two equations, and combining with the flux from Eq. (1) yields a differential equation describing the mass balance between the two chambers

$$\frac{d}{dt}(C_D - C_R) = k_p \tilde{\beta} (C_R - C_D) \quad (3)$$

where

$$\tilde{\beta} = \frac{2A}{V} \quad (4)$$

with initial condition

$$t = 0, \quad C_D - C_R = C_D^0 - C_R^0 \quad (5)$$

where  $C_D^0$  and  $C_R^0$  are initial concentrations in the donor and receptor chamber, respectively. If the receptor chamber is initially filled with pure solvent, then  $C_R^0$  is zero.

Integrating the differential equation subject to this condition gives the desired result:

$$\frac{C_D - C_R}{C_D^0 - C_R^0} = \exp(-k_p \tilde{\beta} t) \quad (6)$$

or

$$k_p \tilde{\beta} t = \ln \left( \frac{C_D^0 - C_R^0}{C_D - C_R} \right) \quad (7)$$

If we assume that  $C_D = C_D^0 - C_R$  and  $C_R^0 = 0$  then

$$k_p \tilde{\beta} t = \ln \left( \frac{C_D^0}{C_D^0 - 2C_R} \right); \quad \tilde{\beta} = \frac{2A}{V}. \quad (8)$$

Thus, the membrane permeance  $k_p$  in RhoB is obtained in this case from the slope of the  $\ln \left( \frac{C_D^0}{C_D^0 - 2C_R} \right)$  vs.  $\tilde{\beta} t$  plot.

The concentration profile versus time is given by

$$C_R = \frac{1}{2}C_D^0[1 - \exp(-k_p\tilde{\beta}t)]. \quad (9)$$

Moreover, for an experiment that does not reach its membrane steady state condition until a known time  $t^{ss}$ , then the conditions at time  $t^{ss}$  are  $C_D^{ss} = C_D^0 - C_R^{ss}$ ;  $C_D = C_D^0 - C_R$ ; and  $C_R^{ss}$  and  $C_R$  are measured. Under these conditions the membrane permeance,  $k_p$ , can be derived from

$$k_p\tilde{\beta}(t - t^{ss}) = \ln\left(\frac{C_D^0 - 2C_R^{ss}}{C_D^0 - 2C_R}\right) \quad (10)$$

and the concentration profile versus time can be obtained from adaptations of the equations above.

## 2.5 Statistical Analysis

A linear mixed model was used to derive membrane permeance,  $k_p$ , from the slope of  $\ln\left(\frac{C_D^0}{C_D^0 - 2C_R}\right)$  versus  $\tilde{\beta}t$ , as defined in Eq. (8) [35]. The fixed effects were: number of holes (categorical), time, and interactions between number of holes and time. A random intercept was included for each experiment run. The interaction between the number of holes and time was examined by using a global likelihood ratio test, comparing the previously mentioned model to one without interaction terms. All permeance values are reported with the standard error derived from the model. A p-value threshold of 0.05 was used for all tests.

## 3 Results

Experimentally measured receptor chamber concentration of RhoB for all experiments, normalized by exposed membrane area, is shown in Fig. 4 and Fig. 5. The maximum concentration of RhoB measured in the receptor chamber at 165 min was  $100.1 \mu\text{M mm}^{-2}$  for experiments using PBS and  $10.5 \mu\text{M mm}^{-2}$  for experiments utilizing P407, corresponding to 9.69% and 0.73% of donor chamber concentration respectively. These concentrations meet the conditions for continuous infinite dosing, as is discussed further in additional analyses in this Appendix [36, 37]. Of note, polymer and copolymer drug carriers with temperature-dependent liquid-gel transitions often release treatment at a high rate in the initial phases before reaching a steady-state rate of material transfer [38]. This effect is known as *burst release* and has previously been documented for P407-based drug formulations [39, 40]. We observed this effect in the initial stages of all P407-based experiments.

To account for the burst release observed in experiments utilizing P407, the data from the first 45 minutes were excluded from the linear mixed models, in accordance with established methods for measuring time of burst release. Predicted concentration curves using these

permeance values were then constructed in accordance with Eq. (9) and are shown overlying the experimental data in the above-mentioned Fig. 4 and Fig. 5. Permeance values,  $k_p$ , for all experiments are reported in Table 2 with standard error. Two measures of statistical significance are included in the analysis: (1) we report p-values for the difference in  $k_p$  between experiments with perforations and experiments of the same delivery substance without perforations; (2), we report p-values for the difference in  $k_p$  between experiments of the same delivery substance with different number of perforations but equivalent perforation cross-sectional areas.

### 3.1 Experiments Utilizing PBS as Solvent

As shown in Table 2, the permeance of RhoB in PBS across an unperforated artificial membrane was  $3.04 \times 10^{-6} \text{ ms}^{-1}$ . The introduction of one or more microperforations was associated with increased permeance of RhoB in PBS across the membrane ( $p < 0.05$ ). The permeance of RhoB in PBS also increased with each additional perforation as well as with greater total perforation cross-sectional area. As hypothesized, there was no difference between the permeance of RhoB in PBS across membranes with equal perforation areas (i.e., four 100  $\mu\text{m}$  perforations and one 200  $\mu\text{m}$  perforation;  $p = 0.627$ ).

### 3.2 Experiments Utilizing P407 as Solvent

The permeance of RhoB in P407 was  $2.2 \times 10^{-7} \text{ ms}^{-1}$  across an unperforated artificial membrane. This permeance is more than an order of magnitude lower than that of RhoB in PBS ( $p < 0.001$ ). The permeance of RhoB in P407 across a membrane with one 200  $\mu\text{m}$  perforation was  $3.0 \times 10^{-7} \text{ ms}^{-1}$ , which is higher than the permeance in an unperforated membrane ( $p < 0.001$ ). In contrast to experiments in PBS, there was a significant difference between the permeance of RhoB in P407 across membranes with equal perforation areas (i.e. four 100  $\mu\text{m}$  perforations and one 200  $\mu\text{m}$  perforation;  $p < 0.002$ ). Moreover, there is no difference in permeance of RhoB in P407 across a membrane with four 100  $\mu\text{m}$  perforations compared to the absence of perforations ( $p = 0.749$ ).

## 4 Discussion

Our study is the first to investigate the role of multiple microscopic perforations as an adjunct to prolonged therapeutic delivery by gelatinous drug carriers. Using an adapted Valia-Chien cell diffusion system, we established a standardized and controlled method for studying the permeance of small molecules across thin anatomic barriers, including but not limited to the RWM. Based on prior work by our laboratory, we expected the introduction of multiple microperforations to enhance diffusive transport across the artificial membrane barrier, regardless of solvent (saline versus P407) [15]. We also compared the effects of perforation size and number of perforations on permeance. This experimental question was guided by clinical concerns; large perforations in the RWM can cause leakage of perilymph from the inner ear, although the exact conditions under which this pathology occurs are experimentally unclear [41]. Small perforations, however, are thought to minimize the risk of outward leakage of perilymph. To this end, we investigated whether many small perforations in the membrane would enhance diffusion to the same degree as one large perforation of equal cross-sectional area.



As expected, in experiments utilizing saline as the solvent for RhoB, we observed an increase in permeance for all perforated membranes, regardless of perforation size or number. Permeance across the membrane also steadily increased with the number of uniformly-sized 100  $\mu\text{m}$  perforations. Of note, we observed no difference in permeance across perforated membranes with equivalent cross-sectional perforation areas. Together, these observations validate our hypotheses and provide a strong basis for predicting diffusion patterns under other conditions. For example, our study used membranes with up to four 100  $\mu\text{m}$  perforations, which resulted in a 1.5-fold increase in measured permeance. Extrapolation of these results would suggest that a three-by-three array of nine perforations representing less than 1% of the total membrane area could more than double the rate of diffusion. This finding, that multiple small perforations can dramatically increase the rate of diffusion across a membrane from a saline reservoir, is highly encouraging for the use of microperforations to enhance diffusive therapy in the ear.

Our experiments utilizing P407 gel as the solvent for RhoB demonstrated a different pattern of diffusion. We observed an initial burst release of solute—a behavior that has frequently been documented in studies of therapies delivered by hydrogel carriers. Of note, the introduction of perforations appeared to enhance the effects of burst release. We propose several explanations for the observed burst release.

First, the initial flux of solute across the membrane is high due to a high concentration of solute dissolved uniformly throughout P407 (Fig. 6). Slow movement of solute through P407 in areas far from the membrane causes delayed repletion of areas immediately adjacent to the membrane. This phenomenon results in a concentration gradient in the P407 gel where the concentration of solute is high in areas far from the membrane, and low in areas near the membrane. Eventually, the concentration gradient of solute in P407 is such that the flux across the membrane reaches a steady state. As a result, in the receptor chamber, we observe an initial high rate of diffusion, with a steady decline until the rate of diffusion reaches a steady state. This phenomenon is likely exacerbated by our inability to stir P407 gel and uniformly disperse the contained solute, unlike in experiments using saline as the solvent.

Second, the initial burst effect is likely compounded by a change in permeance of solute through poloxamer over time due to incomplete setting of the polymer at the start of the experiment. This phenomenon causes immediate release of solute from non-gelified solution (high permeance) and slower release of solute after complete gelification (low permeance).

Overall, the RhoB diffusion rate in P407 after the initial burst release was more than 10 times lower than that in saline. This result is expected, as the polymer matrix formed by gelified P407 slows diffusion. This reduced rate of diffusion and release of solute from P407 has important clinical implications for drug delivery to the inner ear. Current treatment protocols utilizing IT injection require the patient to lie supine for 15 minutes after injection, during which the delivered substance remains in contact with the RWM. Afterwards, the patient sits and the liquid solution delivered with IT is lost via the Eustachian tube. In contrast, P407-based solutions delivered via IT injection reside in the middle ear for one to two weeks, allowing for extended time of drug diffusion. Our results suggest that P407 may require approximately two and a half hours to release the same amount of drug released by

saline in the clinically mandated 15 minutes. Including the effects of burst release, P407 may require even less time, approximately one and a half hours, to deliver the same amount. Over the one to two weeks that P407 remains in the middle ear, the solution could release 50 times the amount of drug released by saline in 15 minutes; however, our study does not cover this extended time frame and further experimentation is necessary to clarify the role of long-term gelatinous drug carriers for inner ear therapy.

Our experiments using P407 as a solvent also demonstrated an unexpected effect of perforations on membrane permeance—while a larger perforation increased the steady state permeance of solute across the membrane, smaller perforations did not have any effect on the steady state rate of diffusion, despite appearing to enhance the initial burst release of RhoB across the membrane. These findings may be explained by diffusion characteristics that are intrinsic to gel-based carriers. For example, the surface tension between the donor P407 gel, the barrier membrane, and the saline within the receptor chamber may prevent diffusion across the system below a critical perforation size. Other interactions between P407 solvent and membrane perforation may also help explain this unexpected finding. Of note, local depletion of solute in the immediate vicinity of a perforation may scale non-linearly with perforation size. Alternatively, using Eq. (1) we can describe the steady state permeance of the total system,  $k_t$ , using the interactions between various components of the system. In this model of our system, the permeance through solvent,  $k_s$ , is in parallel with both the permeance across the membrane,  $k_m$ , excluding the effects of perforations, and the permeance across the perforations,  $k_h$ , in series, such that

$$k_t = \frac{1}{\frac{1}{k_s} + \frac{1}{k_m + k_h}}. \quad (11)$$

Although this model fails to explain why one large perforation would produce different results from four small perforations of equivalent cross-sectional area, it helps to explain why the permeance of solute in P407 with four small perforations is similar to the permeance without perforations: if  $k_s \ll k_m + k_h$ , then the effects of  $k_m + k_h$  are negligible. In this case,  $k_t \approx k_s$ , so the effects of perforations are smaller when using a solvent with a low permeance such as P407. On the contrary, if  $k_s \gg k_m + k_h$ , then  $k_t \approx k_m + k_h$ , so the effects of perforations are larger when using a solvent with higher permeance such as saline. This proposed explanation is consistent with our experiments using saline, as described previously. Lastly, it is possible that longer experimental timescales are necessary to compare the permeance of solute in P407 with four small perforations against the permeance without perforations.

Overall, our experiments in saline suggest that multiple small microperforations are an effective means for enhancing saline-based drug diffusion across thin anatomical membranes, while reducing the risk of clinical complications. Meanwhile, our experiments in P407 provide insight into the complexities of hydrogel-based drug delivery with regards to microperforations—specifically that small 100  $\mu\text{m}$  perforations may have little effect on P407-based drug diffusion and that larger perforations are necessary to increase drug

diffusion rate. Although larger perforations may increase the risk of fluid leakage, in practice, P407, being a viscous gel, likely forms a seal over the perforations. In guinea pigs, hydrogels including P407 were shown to seal RWM perforations after direct intracochlear injections, leading to significantly increased drug retention [42]. These injections involved smaller perforations of 20–40  $\mu\text{m}$  diameter over the course of 40 minutes; the use of P407 to seal a larger perforation and for longer time periods has not been explored [42]. Therefore, it is important to further investigate the properties of P407 drug delivery when coupled with microperforations, such as the minimum microperforation size needed to enhance drug delivery, the maximum microperforation size allowed for clinical safety, the ability of P407 to seal large perforations, and the rate of perforation healing *in vivo*.

## 5 Conclusion

The goal of gel-based delivery vehicles and other continuous release drug formulations is to provide more accurate and precise dosing of therapy. Here we propose an artificial model for testing diffusion of material through anatomical membranes with and without microperforations. Our experiments show that the diffusion of RhoB in saline solution across an artificial membrane increases with larger total cross-sectional area of microperforations applied to the membrane. The diffusion-enhancing effects of microperforations on gel-based drug delivery are more complex and do not scale with total cross-sectional area of microscopic perforations. Diffusion of RhoB in P407 across an artificial membrane increases with a large perforation, but not with multiple small perforations, perhaps due to diffusion characteristics intrinsic to gel-based drug carriers.

## Acknowledgments

We gratefully acknowledge support by the National Institutes of Health (NIH) National Institute on Deafness and Other Communication Disorders (NIDCD) with award number R01DC014547. We thank Hirobumi Watanabe, PhD, for helpful discussions in experimental design, Jimmy K. Duong, MPH, for guidance in developing the linear mixed model used in our analysis, and Miguel Arriaga, PhD, and Arvind Narayanaswamy, PhD, for discussions concerning material diffusion.

## Appendix A Additional Models

Below, we suggest two additional models (Eqs. 16 and 20), each with their own assumptions, that can be used to describe our experiments. Table 3 summarizes the permeances  $k_p$  derived from each of the models. All three models give very similar estimates of the  $k_p$ ; thus, the assumptions for the approaches described in Eqs. 16 and 20 seem to be valid for our experiments.

### A.1 Case I: infinite dosing

In the case that the donor chamber is maintained at a saturated solubility condition with saturated concentration  $C_D^s$ , the pseudo-steady state flux is

$$j_{RhoB}^s = k_p(C_D^s C_R) \quad (12)$$

while the mass balance on the receptor chamber of the Valia-Chien Diffusion Cell is written as

$$V_R \frac{dC_R}{dt} = + A j_{RhoB}^s = k_p A (C_D^s - C_R) \quad (13)$$

with solution

$$C_R = C_D^s - (C_D^s - C_R^0) \exp\left(-\frac{k_p A}{V_R} t\right) \quad (14)$$

or

$$\ln\left(\frac{C_D^s - C_R}{C_D^s - C_R^0}\right) = k_p \frac{A}{V_R} t \quad (15)$$

Since  $C_R^0 = 0$

$$k_p \tilde{\beta} t = \ln\left(\frac{C_D^s}{C_D^s - C_R}\right); \quad \tilde{\beta} = \frac{A}{V_R} \quad (16)$$

## A.2 Case II: infinite dosing for the donor and below sink condition for the receptor

In the case that the donor chamber is maintained at a saturation solubility with concentration  $C_D^s$  and the receptor chamber is maintained below a sink condition such that  $C_R < 10\% C_D^s$ . Then, the pseudo-steady state flux across the membrane can be simplified to

$$j_{RhoB}^{ss} = k_p C_D^s \quad (17)$$

The flux  $j_{RhoB}^{ss}$  represents the amount of RhoB permeating through a unit surface area of the membrane per time. Thus, it can be written as

$$j_{RhoB}^{ss} = \frac{Q_{RhoB}}{A t} \quad (18)$$

$$C_D^s = \frac{Q_D^s}{V_D} \quad (19)$$

Combining equations (17) - (19) yields

$$k_p t = \left( \frac{Q_{Rhob}}{A} \right) / \left( \frac{Q_D^s}{V_D} \right) \quad (20)$$

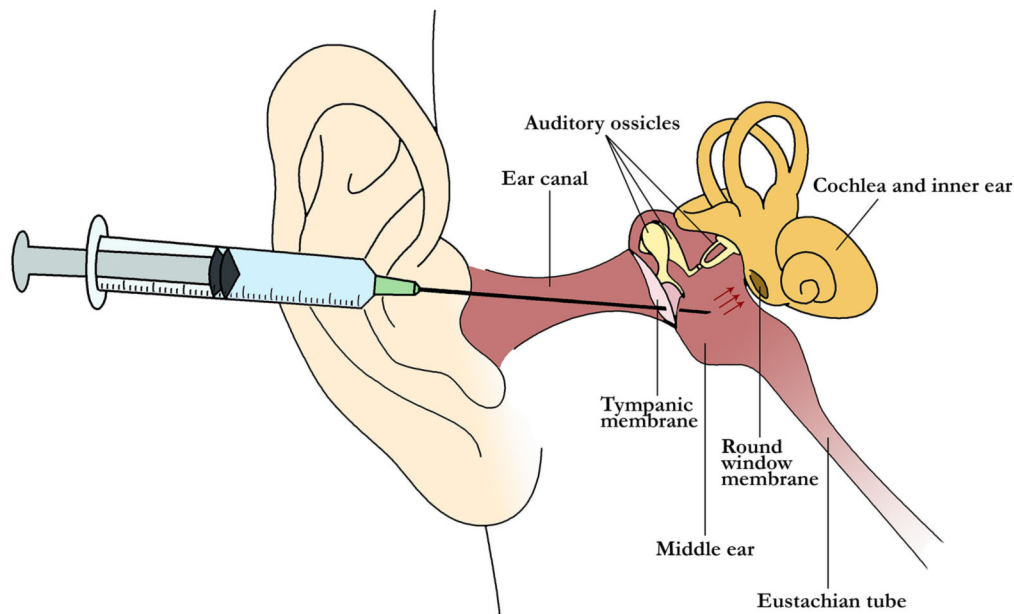
Then, the permeance  $k_p$  is obtained as the slope of the  $\left( \frac{Q_{Rhob}}{A} \right) / \left( \frac{Q_D^s}{V_D} \right)$  versus time  $t$ .

## References

- [1]. Bird PA, Begg EJ, Zhang M, Keast AT, Murray DP, and Balkany TJ. Intratympanic versus intravenous delivery of methylprednisolone to cochlear perilymph. *Otology & Neurotology*, 28(8):1124–30, 2007. PMID: 18043438. [PubMed: 18043438]
- [2]. Blakley BW. Update on intratympanic gentamicin for meniere's disease. *Laryngoscope*, 110(2 Pt 1):236–40, 2000. PMID: 10680922. [PubMed: 10680922]
- [3]. Casani AP, Piaggi P, Cerchiai N, Seccia V, Franceschini SS, and Dallan I. Intratympanic treatment of intractable unilateral meniere disease: gentamicin or dexamethasone? a randomized controlled trial. *Otolaryngology Head & Neck Surgery*, 146(3):430–7, 2012. PMID: 22101095. [PubMed: 22101095]
- [4]. Shemirani NL, Schmidt M, and Friedland DR. Sudden sensorineural hearing loss: An evaluation of treatment and management approaches by referring physicians. *Otolaryngology-Head and Neck Surgery*, 140(1):86–91, 2009. PMID: 19130968. [PubMed: 19130968]
- [5]. Silverstein H, Lewis WB, Jackson LE, Rosenberg SI, Thompson JH, and Hoffmann KK. Changing trends in the surgical treatment of ménière's disease: results of a 10-year survey. *Ear, Nose, & Throat Journal*, 82(3):185–187, 191–194, 2003. PMID: 12696238.
- [6]. Hahn H, Kammerer B, DiMauro A, Salt AN, and Plontke SK. Cochlear microdialysis for quantification of dexamethasone and fluorescein entry into scala tympani during round window administration. *Hearing Research*, 212:236–244, 2006. PMID: 16442251. [PubMed: 16442251]
- [7]. Kim M, Hee Do K, and Kim KS. Isosorbide concentration in perilymph of the guinea pig after oral administration versus that after round window perfusion. *Clinical and Experimental Otorhinolaryngology*, 7(4):281–285, 2014. PMID: 25436047. [PubMed: 25436047]
- [8]. Goycoolea MV, Muchow D, and Schachern P. Experimental studies on round window structure: function and permeability. *Laryngoscope*, 98:1–20, 1988. PMID: 3287079.
- [9]. Goycoolea MV. Clinical aspects of round window membrane permeability under normal and pathological conditions. *Acta Oto-Laryngologica*, 121:437–447, 2001. PMID: 11508501. [PubMed: 11508501]
- [10]. Plontke SK, Mynatt R, Gill RM, Borgmann S, and Salt AN. Concentration gradient along the scala tympani after local application of gentamicin to the round window membrane. *Laryngoscope*, 117:1191–1198, 2007. PMID: 17603318. [PubMed: 17603318]
- [11]. Salt AN and Ma Y. Quantification of solute entry into cochlear perilymph through the round window membrane. *Hearing Research*, 154:88–97, 2001. PMID: 11423219. [PubMed: 11423219]
- [12]. Li Lihua, Ren Jihao, Yin Tuanfang, and Liu Wei. Intratympanic dexamethasone perfusion versus injection for treatment of refractory sudden sensorineural hearing loss. *European Archives of Oto-Rhino-Laryngology*, 270(3):861–867, 3 2013. [PubMed: 22669272]

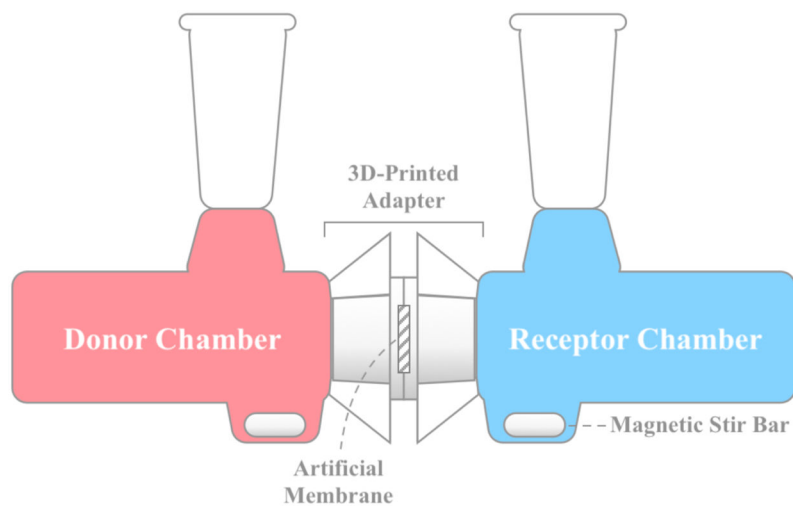
- [13]. Hoffer Michael E., Allen Keith, Kopke Richard D., Weisskopf Peter, Gottshall Kim, and Wester Derin. Transtympanic Versus Sustained-Release Administration of Gentamicin: Kinetics, Morphology, and Function. *The Laryngoscope*, 111(8): 1343–1357, 8 2001. [PubMed: 11568567]
- [14]. Mikulec Anthony A., Hartssock Jared J., and Salt Alec N.. Permeability of the Round Window Membrane Is Influenced by the Composition of Applied Drug Solutions and by Common Surgical Procedures. *Otology & Neurotology*, 29(7):1020–1026, 10 2008. [PubMed: 18758387]
- [15]. Kelso CM, Watanabe H, Wazen JM, Bucher T, Qian ZJ, Olson ES, Kysar JW, and Lalwani AK. Microperforations significantly enhance diffusion across round window membrane. *Otology & Neurotology*, 36(4):694–700, 04 2015. [PubMed: 25310125]
- [16]. Watanabe H, Kysar JW, and Lalwani AK. Microanatomic analysis of the round window membrane by white light interferometry and microcomputed tomography for mechanical amplification. *Otology & Neurotology*, 35(4):672–678, 2014. [PubMed: 24622022]
- [17]. Watanabe H, Kysar JW, and Lalwani AK. Round window membrane as a portal for inner ear therapy In Lalwani AK and Pfister MHF, editors, *Recent Advances in Otolaryngology Head & Neck Surgery*, volume 6, chapter 2, pages 39–56. JP Medical Publishers, London, 2017.
- [18]. Aksit Aykut, Arteaga Daniel N., Arriaga Miguel, Wang Xun, Watanabe Hirobumi, Kasza Karen E., Lalwani Anil K., and Kysar Jeffrey W.. In-vitro perforation of the round window membrane via direct 3-d printed microneedles. *Biomedical Microdevices*, 20(2):47, 6 2018. [PubMed: 29884927]
- [19]. Stevens JP, Watanabe H, Kysar JW, and Lalwani AK. Serrated needle design facilitates precise round window membrane perforation. *Journal of Biomedical Materials Research: Part A*, 104(7): 1633–1637, 2016. [PubMed: 26914984]
- [20]. Wazen JM, Stevens JP, Watanabe H, Kysar JW, and K Lalwani A. Silver/silver chloride microneedles can detect penetration through the round window membrane. *Journal of Biomedical Materials Research Part B: Applied Biomaterials*, 105(2):307–311, 2017. [PubMed: 26506512]
- [21]. Watanabe H, Cardoso L, Lalwani AK, and Kysar JW. A dual wedge microneedle for sampling of perilymph solution via round window membrane. *Biomedical Microdevices*, 18(2):1–8, 2016. [PubMed: 26660457]
- [22]. Cai Hui, Liang Zhongping, Huang Wenli, Wen Lu, and Chen Gang. Engineering plga nano-based systems through understanding the influence of nanoparticle properties and cell-penetrating peptides for cochlear drug delivery. *International Journal of Pharmaceutics*, 532(1):55–65, 2017. [PubMed: 28870763]
- [23]. Salt Alec N, Hartssock Jared, Plontke Stefan, LeBel Carl, and Piu Fabrice. Distribution of dexamethasone and preservation of inner ear function following intratympanic delivery of a gel-based formulation. *Audiology & Neurotology*, 16(5):323–335, 07 2011. [PubMed: 21178339]
- [24]. Wang X, Dellamary L, Fernandez R, Ye Q, LeBel C, and Piu F. Principles of inner ear sustained release following intratympanic administration. *Laryngoscope*, 121(2):385–391, 2011. PMID: 21271594. [PubMed: 21271594]
- [25]. Wang X, Dellamary L, Fernandez R, Harrop A, Keithley EM, Harris J, Ye Q, Lichter J, LeBel C, and Piu F. Dose-dependent sustained release of dexamethasone in inner ear cochlear fluids using a novel local delivery approach. *Audiology & Neuro-Otology*, 14:393–401, 11 2009. [PubMed: 19923809]
- [26]. Le Ray AM, Iooss P, Gouyette A, Vonarx V, Patrice T, and Merle C. Development of a “continuous-flow adhesion cell” for the assessment of hydrogel adhesion. *Drug Development and Industrial Pharmacy*, 25(8):897–904, 1999. PMID: 10434133. [PubMed: 10434133]
- [27]. Dumortier Gilles, Grossiord Jean Louis, Agnely Florence, and Chaumeil Jean Claude. A review of poloxamer 407 pharmaceutical and pharmacological characteristics. *Pharmaceutical Research*, 23(12):2709–2728, 2006. [PubMed: 17096184]
- [28]. Akkari ACS, Papini JZB, Garcia GK, Franco MKKD, Cavalcanti LP, Gasperini A, Alkschbirs MI, Yokaichyia F, de Paula E, Tófoli GR, and de Araujo DR. Poloxamer 407/188 binary thermosensitive hydrogels as delivery systems for infiltrative local anesthesia: Physico-chemical characterization and pharmacological evaluation. *Materials Science and Engineering C*, 68:299–307, 2016. PMID: 27524024. [PubMed: 27524024]

- [29]. Engleder Elisabeth, Honeder Clemens, Klobasa Julia, Wirth Michael, Arnoldner Christoph, and Gabor Franz. Preclinical evaluation of thermoreversible triamcinolone acetonide hydrogels for drug delivery to the inner ear. *International Journal of Pharmaceutics*, 471(1):297–302, 2014. [PubMed: 24907595]
- [30]. Mair EA, Park AH, Don D, Koempel J, Bear M, and LeBel C. Safety and efficacy of intratympanic ciprofloxacin otic suspension in children with middle ear effusion under-going tympanostomy tube placement: Two randomized clinical trials. *JAMA Otolaryngology Head Neck Surgery*, 142(5):444–51, 2016. PMID: 26985629. [PubMed: 26985629]
- [31]. Environmental Protection Agency. Recommended protocol for in vitro percutaneous absorption rate studies. *Federal Register Notices*, 61(65):14773–14778, 1996. Agency Docket: OPPTS-42186A.
- [32]. Tamura T, Kita T, Nakagawa T, Endo T, Kim TS, Ishihara T, Mizushima Y, Higaki M, and Ito J. Drug delivery to the cochlea using plga nanoparticles. *Laryngoscope*, 115(11):2000–2005, 2005. PMID: 16319613. [PubMed: 16319613]
- [33]. Chien Yie W. and Valia Kirti H.. Development of a dynamic skin permeation system for long-term permeation studies. *Drug Development and Industrial Pharmacy*, 10(4):575–599, 1984.
- [34]. Cussler EL. *Diffusion Mass Transfer in Fluid Systems*. Cambridge University Press, UK, 2009.
- [35]. Bonate PL. *Linear Mixed Effects Models*, pages 181–204. Springer US, Boston, MA, 2006.
- [36]. OECD. Test no. 428: Skin absorption: In vitro method. OECD Publishing, 2004.
- [37]. Selzer Dominik, Abdel-Mottaleb Mona M.A., Tsambika Hahn, Schaefer Ulrich F., and Dirk Neumann. Finite and infinite dosing: Difficulties in measurements, evaluations and predictions. *Advanced Drug Delivery Reviews*, 65(2):278–294, 2013. [PubMed: 22750806]
- [38]. Huang X and Brazel CS. On the importance and mechanisms of burst release in matrix-controlled drug delivery systems. *Current Drug Delivery*, 73(2–3): 121–36, 2001. PMID: 11516493.
- [39]. Shau PA, Dangre PV, and Potnis VV. Formulation of thermosensitive in situ otic gel for topical management of otitis media. *Indian Journal of Pharmaceutical Sciences*, 77(6):764–770, 2015. PMID: 26997706. [PubMed: 26997706]
- [40]. Alexander A, Saraf S, and Saraf S. Understanding the role of poloxamer 407 based thermoreversible in situ gelling hydrogel for delivery of pegylated melphalan conjugate. *Current Drug Delivery*, 13(4):621–30, 2016. PMID: 26845559. [PubMed: 26845559]
- [41]. Salt AN, Sirjani DB, Hartsock JJ, Gill RM, and Plontke SK. Marker retention in the cochlea following injections through the round window membrane. *Hearing Research*, 232(1–2):78–86, 2007. PMID: 17662546. [PubMed: 17662546]
- [42]. Plontke SK, Hartsock JJ, Gill RM, and Salt AN. Intracochlear drug injections through the round window membrane: Measures to improve drug retention. *Audiology and Neurotology*, 21(2):72–79, 2016. PMID: 26905306. [PubMed: 26905306]

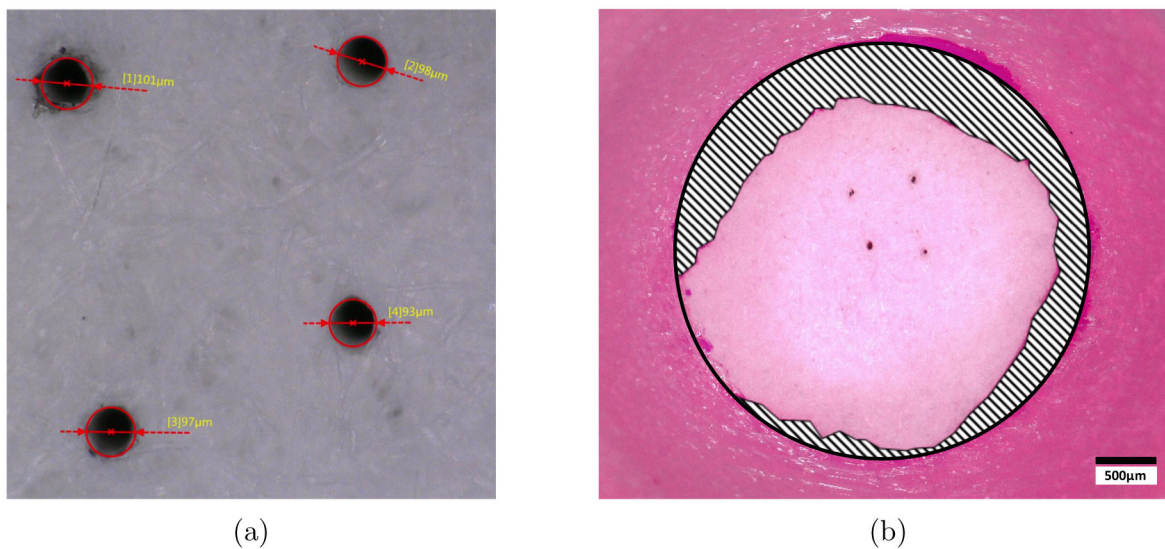


**Figure 1:** Schematic of intratympanic injection: Drug is delivered using a syringe needle via the ear canal, through the tympanic membrane, and into the middle ear space. This space contains the auditory ossicles. The drug diffuses across the round window membrane (red arrows) to enter the cochlea and treat inner ear disease. This liquid therapy can be lost via the Eustachian tube due to gravity when the patient sits upright.



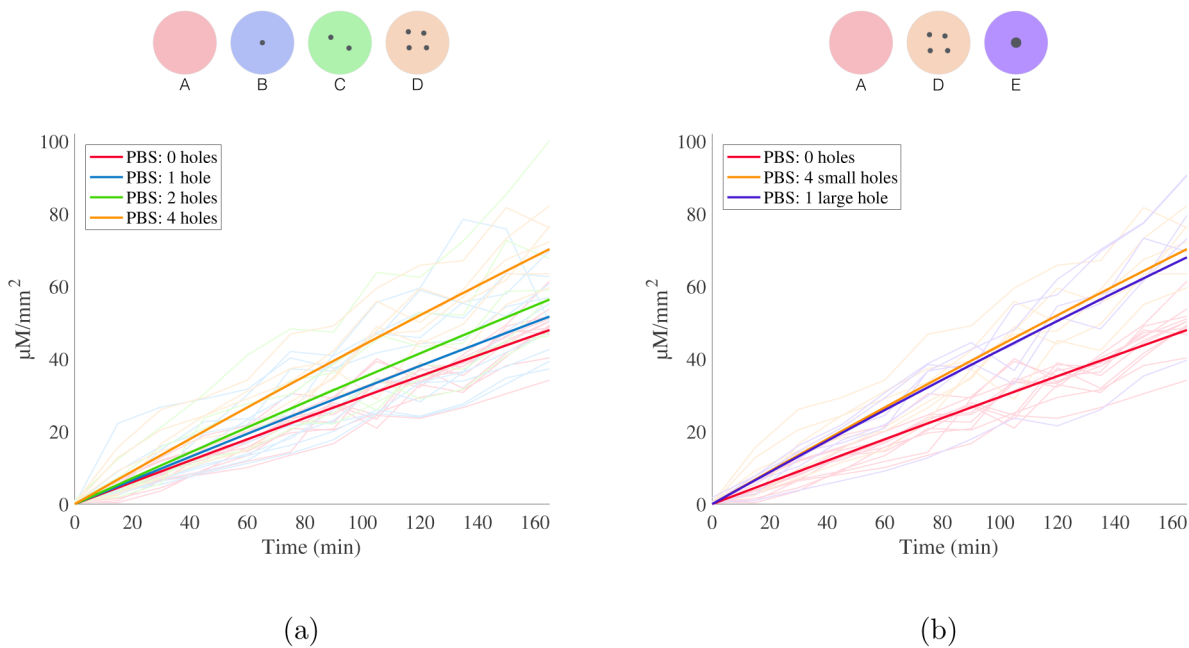


**Figure 2:** Horizontal diffusion cell apparatus: 0.1 mM RhoB in either PBS or P407 was loaded into the donor chamber. Samples drawn from the receptor chamber were used to quantify the diffusion of RhoB across the artificial membrane, which was housed in a 3D-printed adapter. Stirring could not be performed in the donor chamber for experiments utilizing P407 as the solvent.

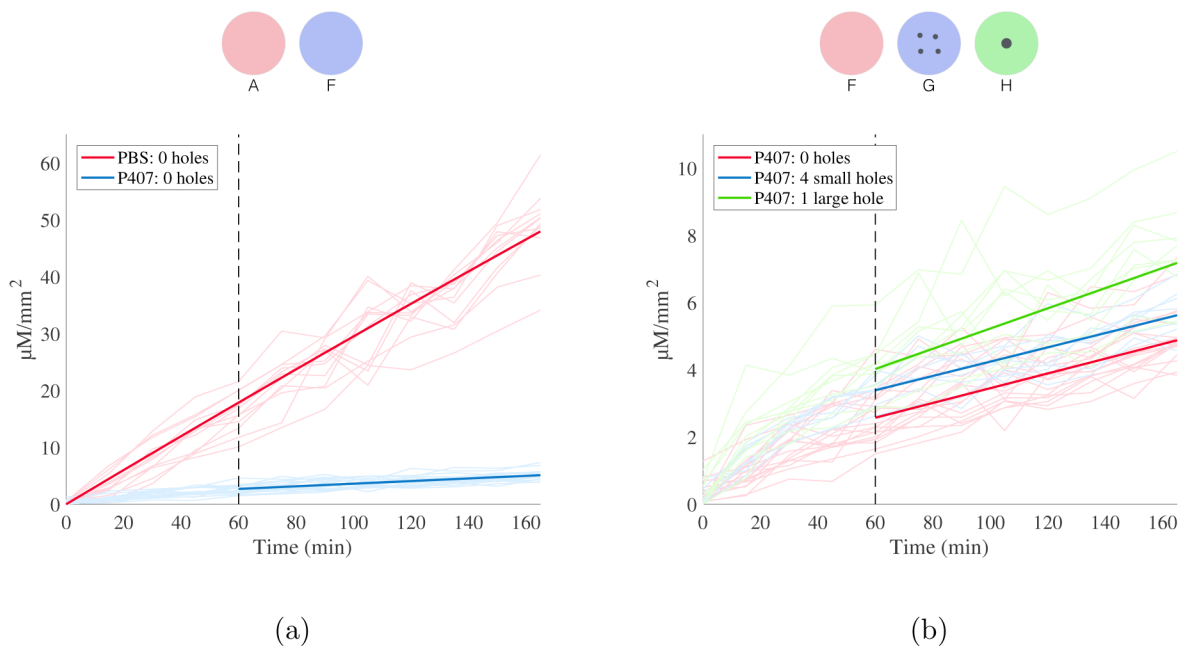


**Figure 3:**

(a) Confirming presence and size of perforations in the filter paper membrane: Whatman™ filter paper with four 100 μm-diameter perforations. Imaging was performed using Keyence VHX-5000 Digital Microscope (Keyence Corporation of America, Elmwood Park, NJ, USA). (b) Measuring membrane area within diffusion cell adapter: Whatman™ filter paper (large circle) with four 100 μm-diameter perforations (small dark dots). Epoxy (shaded) can be seen leaking circumferentially from the edge of the 3D-printed diffusion cell adapter. Exposed filter paper (light pink) was included in the area measurement, while the area covered by epoxy was excluded.

**Figure 4:**

Diffusion of RhoB in PBS. All data is depicted as RhoB concentration in the receptor chamber, normalized by membrane area, as a function of time. Results are color-coded by experiment type, as indicated by legend and above schematic. (a) Predicted concentration profiles for 0, 1, 2 and 4 holes of 100  $\mu\text{m}$  diameter (solid lines), along with raw data (transparent lines). 34 total experiments represented. (b) Predicted concentration profiles for experiments utilizing holes with the same total cross sectional area (one hole 200  $\mu\text{m}$  diameter, four holes 100  $\mu\text{m}$  diameter) with raw data. 24 total experiments represented.

**Figure 5:**

Diffusion of RhoB in P407. All data is depicted as RhoB concentration in the receptor chamber, normalized by membrane area, as a function of time. Results are color-coded by experiment type, as indicated by legend and above schematic. (a) Predicted concentration profiles for 0 holes (solid lines), along with raw data shown (transparent lines). 32 total experiments represented. (b) Diffusion of RhoB in P407. Predicted concentration profiles for holes with same total cross sectional area (one hole 200  $\mu\text{m}$  diameter, four holes 100  $\mu\text{m}$  diameter) in P407 with raw data. 38 total experiments represented.

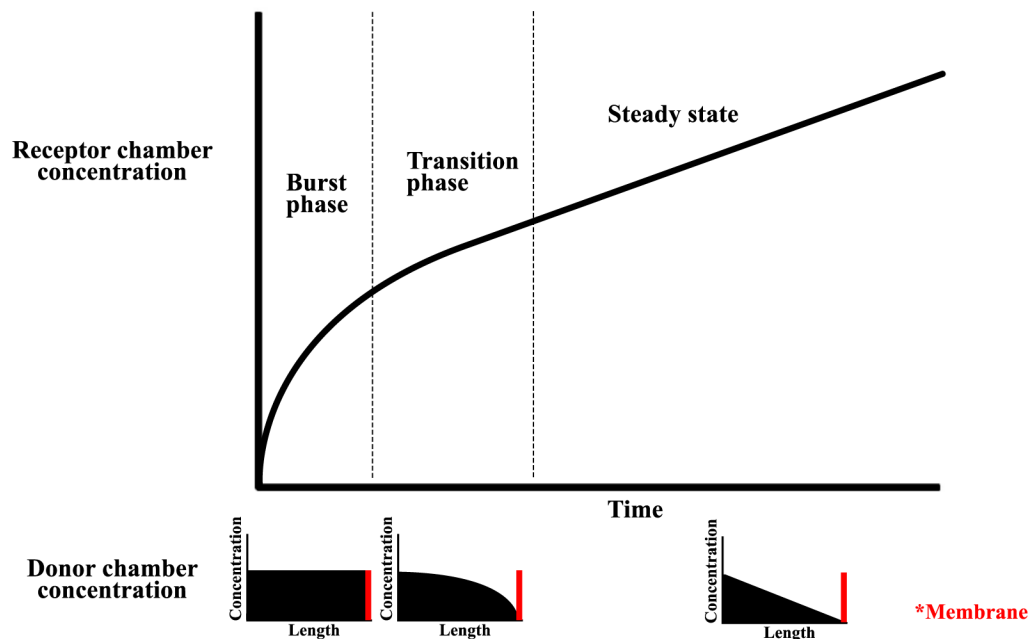


**Figure 6:**

Phases of burst release in receptor chamber shown with corresponding solute concentrations in donor chamber. During initial burst release, a high concentration of solute is dissolved uniformly in the P407 donor chamber. During the transition phase, local depletion occurs in areas near the membrane (red). Afterwards, the flux across the membrane reaches its steady state condition.

**Table 1:**

Summary of Experimental Characteristics by Delivery Substance and Microperforation(s)

Experiment Type	Solvent	Number of Holes	Perforation Diameter ( $\mu\text{m}$ )	Calc. Perf. Area ( $\text{mm}^2$ )	Avg. Membrane Area ( $\text{mm}^2$ )
A	PBS	0	-	-	7.06
B	PBS	1	100	$7.854 \times 10^{-3}$	8.20
C	PBS	2	100	$1.571 \times 10^{-2}$	7.49
D	PBS	4	100	$3.142 \times 10^{-2}$	8.13
E	PBS	1	200	$3.142 \times 10^{-2}$	9.37
F	18% P407	0	-	-	7.33
G	18% P407	4	100	$3.142 \times 10^{-2}$	6.63
H	18% P407	1	200	$3.142 \times 10^{-2}$	6.59

Experiments with different characteristics are organized by type (A through H). Perforation area was calculated assuming circular perforations. Average membrane area was calculated using mean data from original MATLAB code.

Author Manuscript

Author Manuscript

Author Manuscript

Author Manuscript

**Table 2:**

Effects of solvent and microperforation(s) on permeance to Rhodamine B

Experiment Type	Solvent	Number of Holes	Perforation Diameter ( $\mu\text{m}$ )	$k_p$ ( $10^{-6}$ m/s)	p-value*	p-value**
A	PBS	0	-	$3.04 \pm 0.09$	-	
B	PBS	1	100	$3.31 \pm 0.13$	0.037	
C	PBS	2	100	$3.61 \pm 0.15$	<0.001	
D	PBS	4	100	$4.58 \pm 0.15$	<0.001	0.627
E	PBS	1	200	$4.47 \pm 0.15$	<0.001	
F	18% P407	0	-	$0.22 \pm 0.01$	-	
G	18% P407	4	100	$0.22 \pm 0.02$	0.749	<0.002
H	18% P407	1	200	$0.30 \pm 0.02$	<0.001	

\* p-values for the difference in  $k_p$  between experiments with perforations and experiments of the same delivery substance without perforations (i.e., A versus B though E; F versus G and H).

\*\* p-values for the difference in  $k_p$  between experiments of the same delivery substance with perforations of equivalent cross-sectional areas (i.e., D versus E; G versus H).

**Table 3:**

Comparison of  $k_p$  ( $10^{-6}$  m/s) estimates between the three models. (%) Error is shown, using Eq. (8) as a reference.

Experiment Type	$k_p$ from Eq. (8)	$k_p$ from Eq. (16)	(%) Error	$k_p$ from Eq. (20)	(%) Error
A	3.04	2.98	1.97	3.13	2.96
B	3.31	3.22	2.72	3.37	1.81
C	3.61	3.52	2.49	3.90	8.03
D	4.58	4.42	3.49	4.59	0.22
E	4.47	4.30	3.80	4.70	5.15
F	0.22	0.21	4.55	0.21	4.55
G	0.22	0.22	0.00	0.21	4.55
H	0.30	0.28	6.67	0.28	6.67

Author Manuscript

Author Manuscript

Author Manuscript

Author Manuscript